The emerging role of mesenchymal stem cell–derived extracellular vesicles to ameliorate hippocampal NLRP3 inflammation induced by binge-like ethanol treatment in adolescence

Susana Mellado[1], María José Morillo-Bargues[1], Carla Perpiñá-Clérigues[1, 2], Francisco García-García[2], Victoria Moreno-Manzano[3], Consuelo Guerri[1], María Pascual[1, *]

https://doi.org/10.4103/NRR.NRR-D-23-01397

Date of submission: June 18, 2023

Date of decision: October 25, 2023

Date of acceptance: November 13, 2023

Date of web publication: June 24, 2024

From the Contents

Graphical Abstract

Schematic representation of the protective effects of MSC-EVs administration on ethanol-induced hippocampal neuroinflammation by inhibiting NLRP3 inflammasome activation

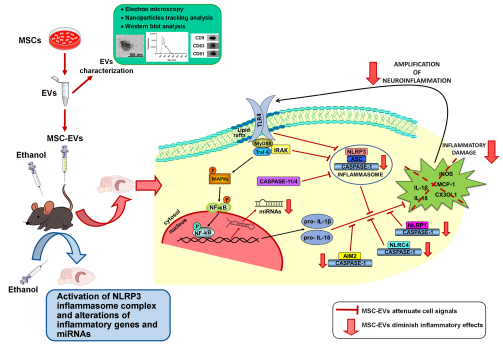

Abstract

Our previous studies have reported that activation of the NLRP3 (NOD-, LRR- and pyrin domain-containing protein 3)-inflammasome complex in ethanol-treated astrocytes and chronic alcohol-fed mice could be associated with neuroinflammation and brain damage. Mesenchymal stem cell-derived extracellular vesicles (MSC-EVs) have been shown to restore the neuroinflammatory response, along with myelin and synaptic structural alterations in the prefrontal cortex, and alleviate cognitive and memory dysfunctions induced by binge-like ethanol treatment in adolescent mice. Considering the therapeutic role of the molecules contained in mesenchymal stem cell-derived extracellular vesicles, the present study analyzed whether the administration of mesenchymal stem cell-derived extracellular vesicles isolated from adipose tissue, which inhibited the activation of the NLRP3 inflammasome, was capable of reducing hippocampal neuroinflammation in adolescent mice treated with binge drinking. We demonstrated that the administration of mesenchymal stem cell-derived extracellular vesicles ameliorated the activation of the hippocampal NLRP3 inflammasome complex and other NLRs inflammasomes (e.g., pyrin domain-containing 1, caspase recruitment domain-containing 4, and absent in melanoma 2, as well as the alterations in inflammatory genes (interleukin-1β, interleukin-18, inducible nitric oxide synthase, nuclear factor-kappa B, monocyte chemoattractant protein-1, and C–X3–C motif chemokine ligand 1) and miRNAs (*miR-21a-5p*, *miR-146a-5p*, and *miR-141-5p*) induced by binge-like ethanol treatment in adolescent mice. Bioinformatic analysis further revealed the involvement of *miR-21a-5p* and *miR-146a-5p* with inflammatory target genes and NOD-like receptor signaling pathways. Taken together, these findings provide novel evidence of the therapeutic potential of MSC-derived EVs to ameliorate the hippocampal neuroinflammatory response associated with NLRP3 inflammasome activation induced by binge drinking in adolescence.

Key Words: adolescence; binge-like ethanol treatment; extracellular vesicles; hippocampus; mesenchymal stem cells; neuroinflammation; NOD-, LRR- and pyrin domain-containing protein 3 (NLRP3)

Introduction

Nucleotide-binding oligomerization domain (NOD)-like receptors (NLRs) are one of the main signals of innate immune sensors, delivering immediate responses against tissue injury, pathogenic invasion, and stress conditions. The NLRs family is activated through the recognition of both pathogen-associated molecular patterns and damage-associated molecular patterns in the host cytosol (Almeida-da-Silva et al., 2023). Several

[1]Department of Physiology, School of Medicine and Dentistry, University of Valencia, Valencia, Spain; [2]Bioinformatics and Biostatistics Unit, Príncipe Felipe Research Center, Valencia, Spain; [3]Neuronal and Tissue Regeneration Laboratory, Príncipe Felipe Research Center, Valencia, Spain
*__Correspondence to:__ María Pascual, PhD, maria.pascual@uv.es.
https://orcid.org/0000-0003-1420-631X (María Pascual)

Funding: *This work was supported by grants from the Spanish Ministry of Health-PNSD (2019-I039 and 2023-I024) (to MP); FEDER/Ministerio de Ciencia e Innovación – Agencia Estatal de Investigación PID2021-1243590B-I100 (to VMM); GVA (CIAICO/2021/203) (to MP); the Primary Addiction Care Research Network (RD21/0009/0005) (to MP); and a predoctoral fellowship from the Generalitat Valenciana (ACIF/2021/338) (to CPC).*

How to cite this article: *Mellado S, Morillo-Bargues MJ, Perpiñá-Clérigues C, García-García F, Moreno-Manzano V, Guerri C, Pascual M (2025) The emerging role of mesenchymal stem cell–derived extracellular vesicles to ameliorate hippocampal NLRP3 inflammation induced by binge-like ethanol treatment in adolescence. Neural Regen Res 20(4):1153-1163.*

members of the NLR family have been identified, such as pyrin domain-containing 1 (NLRP1), NOD-, LRR- and pyrin domain-containing protein 3 (NLRP3), caspase recruitment domain-containing 4 (NLRC4), and a member of the PYHIN protein family absent in melanoma 2 (AIM2). The activation of NLRs is capable of forming inflammasomes, which are multiprotein complexes that activate caspase-1, leading to the processing and secretion of the pro-inflammatory cytokines interleukin-1β (IL)-1β and IL-18 (Almeida-da-Silva et al., 2023).

Among NLRs, NLRP3 is currently the most fully described inflammasome and plays a vital role in the innate immune system. In response to microbial infection and cellular damage, it mediates caspase-1 activation and the release of proinflammatory cytokines, IL-1β/IL-18. It consists of the NLRP3 scaffold, adaptor apoptosis-associated speck-like protein containing a CARD (ASC), and caspase-1 (Almeida-da-Silva et al., 2023). The activation of these receptors triggers an immune response activation and tissue repair processing. However, abnormalities in any of these inflammasome receptors may cause uncontrolled inflammation due to either sustained compensatory adaptive immune activation or hyper-responsive innate immune signaling (Wang and Hauenstein, 2020; Piancone et al., 2021). Our previous studies demonstrated that, in both cultured astroglial cells and in cerebral cortices of wild-type (WT) mice, triggering caspase-1 activation and the induction of IL1β and IL-18. This, in turn, leads to neuroinflammation and brain damage (Alfonso-Loeches et al., 2014, 2016; Montesinos et al., 2016).

One of the most crucial brain regions to develop during adolescence is the hippocampus, which is particularly susceptible to the negative effects of binge ethanol consumption in both humans (Quigley and Committee on Substance Use and Prevention, 2019) and rodent adolescents (Mira et al., 2019). Our previous studies have demonstrated that exposure to binge-like ethanol during adolescence can activate innate immune receptor Toll-like receptor 4 (TLR4) in glial cells. This activation can lead to the release of cytokines and chemokines, causing neuroinflammation and neural damage (Guerri and Pascual, 2019). Activation of the TLR4 response has also been associated with memory and learning dysfunction induced by binge drinking in adolescent mice (Montesinos et al., 2015). Notably, our findings have demonstrated that the extracellular vesicles (EVs) derived from mesenchymal stem cells (MSC-EVs) restore the neuroinflammatory response, along with myelin and synaptic structural alterations in the prefrontal cortex. Additionally, they can alleviate cognitive and memory dysfunctions induced by binge-like ethanol treatment in adolescent mice (Mellado et al., 2023).

Therefore, by considering the therapeutic role of the molecules contained in the MSC-EVs, which play a significant role in both physiological and pathological conditions (e.g., neurodegenerative diseases) (Yin et al., 2019), the present study provides evidence that the administration of MSC-EVs ameliorates the NLRP3 inflammasome-mediated neuroinflammation and inflammation-related genes and microRNAs (miRNAs) in the hippocampus. Notably, these alterations were associated with cognitive impairments in adolescent mice with binge-like ethanol treatment (Montesinos et al., 2015; Pascual et al., 2021; Mellado et al., 2023).

Methods

Adipose tissue processing and culture of MSCs

During knee prosthesis operations on four female patients (aged 50–72 years) under sterile conditions, excess fat tissue was harvested to generate human adipose tissue. Anonymization was applied to the human samples. The Code of Practice 2014/01 (approved on January 4, 2014) was followed by the Regional Ethics Committee for Clinical Research with Medicines and Health Products when evaluating and authorizing the experimental protocol. This study was conducted in accordance with the 1964 *Declaration of Helsinki*, as revised in 2013. No samples were taken from patients who had a history of cancer or bacterial or viral infections at the time of surgery as an exclusion criterion. An informed consent form enabling the use of the adipose samples was willingly signed by each patient. Within 24 hours following extraction, adipose tissue was transferred from the operating room at 4°C in a sterile solution and brought to the laboratory. To clean the tissue and get rid of any leftover blood, each sample was carefully washed several times using PBS plus antibiotics. Then, the adipose tissue was put into sterile Petri dishes (10 g of adipose tissue per 100 mm Petri dish), and it was put in a solution that contained PBS, collagenase type I-A (0.07%, Sigma, St. Louis, MO, USA), dispase I (0.2 mM, Sigma), 100 U/mL penicillin, and 100 µg/mL streptomycin (Gibco, Carlsbad, CA, USA). Using sterile surgical scissors, the adipose tissue was manually cut into small pieces in a laminar flow hood. It was then transferred to a cell flask and left overnight to be digested at 37°C, 20% O_2, and 5% CO_2. The digested adipose tissue was collected the next day and repeatedly centrifuged in PBS containing antibiotics to wash it several times. After centrifuging the cell pellet at 100,000 × *g* for 1 hour, the pellet was again suspended in growth medium, which contained DMEM high glucose (Cytiva Hyclone, Marlborough, MA, USA), 20% FBS (Merck, Darmstadt, Germany), 100 U/mL penicillin, 100 µg/mL streptomycin (Gibco), and 2 mM L-glutamine (Lonza, Walkersville, MD, USA). Upon replacing the medium with a new one the following day, the attached cells were permitted to proliferate until they were almost confluent. The characteristics and descriptions of adipose-derived MSCs have already been published (Mellado-López et al., 2017; Muñoz-Criado et al., 2017).

Isolation of MSC-EVs

A growth medium was used to incubate subconfluent MSCs for 2 days. After that, 100 mL of the media were gathered and centrifuged at 300 × *g* for 10 minutes and the supernatant at 2000 × *g* for 10 minutes, respectively, to remove any detached cells and cell fragments. Apoptotic bodies and other cellular debris were then pelleted by centrifuging the resultant supernatant for 30 minutes at 10,000 × *g*. Next, for 1 hour, EVs were pelleted from the preceding supernatant at 100,000 × *g*. After a PBS wash, the EVs pellet was centrifuged for 1 hour at 100,000 × *g*. Then, EVs were finally suspended in 100 µL PBS

(equivalent to 160 µg of total protein as determined by the BCA protein assay) and diluted to a final concentration of 50 µg/100 µL, and then stored at –80°C.

Animals and treatments

Thirty-two female C57BL/6 WT mice obtained from Harlan Ibérica (Barcelona, Spain) on postnatal day (PND) 30 of age (~14 g of body weight and specific-pathogen-free grade) were used in this study. Mice were kept in cages with three to four animals each, and they were fed a solid diet and water *ad libitum*. All of the environmental factors of the animals, including the cycles of light and dark (12/12 hours), temperature (23°C), and humidity (60%), were regulated. The Ethical Committee of Animal Experimentation of the Príncipe Felipe Research Centre (Valencia, Spain) and the Generalitat Valenciana approved the animal experiments on August 8, 2020 (Project identification code: 2020/VSC/PEA/0145). The animal experiments were conducted in accordance with the guidelines set out in the European Community Council Directive (2010/63/ECC) and Spanish Royal Decree 53/2013 modified by Spanish Royal Decree 1386/2018. Since our earlier research revealed that adolescent females had a greater neuroinflammatory response than adolescent males (Pascual et al., 2017), female mice were used in this study.

According to a study by Brust et al. (2015), the intermittent ethanol treatment was started on PND30, either early in adolescence or during the prepubescent phase. Three-day-old mice (PND30 to PND43) were given intraperitoneally morning doses of either saline or 25% (v/v) ethanol (3 g/kg) in isotonic saline at 2 consecutive days with 2-day gaps without injections for 2 weeks (Pascual et al., 2007; Montesinos et al., 2015). Consistent with a previous study utilizing intraperitoneal ethanol administration (Allen-Worthington et al., 2015), no symptoms of peripheral inflammation, pain, discomfort, or irritation of the peritoneal cavity caused by the intraperitoneal ethanol concentration were observed. Following a single injection of ethanol, blood alcohol levels gradually decreased for 5 hours after reaching their peak in 30 minutes (~340 mg/dL). Animals were also given MSC-EVs (50 µg/dose) or saline (sodium chloride, 0.9%) in the tail vein once a week (with the third and seventh ethanol dose) 3 hours prior to ethanol administration. The treatments that the animals received were divided into four groups at random: 1) physiological saline or control; 2) physiological saline plus MSC-EVs; 3) ethanol; and 4) ethanol plus MSC-EVs. During the intermittent treatment, there were no changes seen in the animals' body or brain weight (Mellado et al., 2023). Twenty-four hours following the eighth and final ethanol or saline administration, the animals (PND 44) were anesthetized by an intraperitoneal injection of sodium penthobarbital (60 mg/kg) (Vetoquinol, Lure, France) and were sacrificed by cervical dislocation to remove the brains. Then, we performed the hippocampus (n = 8 mice/group) dissection with two spatulas, separating the cortex overlying the dorsal hippocampus (Sultan, 2013; Harris et al., 2019; Le Merre et al., 2021; Jaszczyk et al., 2022), and they were stored at –80°C until used.

MSC-EVs characterization by transmission electron microscopy

EVs were prepared according to the methods described in Ibáñez et al. (2019). The Morada digital camera (Olympus Soft Image Solutions GmbH, Münster, Germany) was used to examine the preparations using a transmission FEI Tecnai G2 Spirit electron microscope (FEI Europe, Eindhoven, the Netherlands).

Nanoparticle tracking analysis

The NanoSight NS300 Malvern (NanoSight Ltd., Minton Park, UK) was used to analyze the concentration and absolute size range of the microvesicles, following the methods described in Ibáñez et al. (2019). Following Brownian motion and the diffusion coefficient, particles were automatically tracked and sized. After isolating the MSC-EVs in 100 µL PBS, 1 µL of EVs was resuspended in 1 mL of 0.22 µm-filtered PBS for measurement in the NanoSight. For the nanoparticles tracking analysis, the following parameters were measured: temperature = 25 ± 0.5°C, viscosity = (9.9 ± 0.1) × 10^{-4} Pa·s, frames per second = 25, and measurement time = 30 seconds. All of the samples had the same detection threshold. The total number of particles obtained from the 100 mL of cell media was 209 × 10^{9} particles.

Western blot analysis

The Western blot technique was used on MSC-EVs for their characterization purposes and on hippocampal tissue, following previously mehtods (Montesinos et al., 2015). The primary antibodies employed were: anti-CD9 (rabbit, 1:500, Santa Cruz Biotechnology, Dallas, TX, USA, Cat# sc-9148, RRID: AB_2075905), anti-CD63 (rabbit, 1:500, Santa Cruz Biotechnology, Cat# sc-15363, RRID: AB_648179), anti-CD81 (rabbit, 1:2000, Santa Cruz Biotechnology, Cat# sc-9158, RRID: AB_638255) and anti-calnexin (rabbit, 1:1000, Santa Cruz Biotechnology, Cat# sc-23954, RRID: AB_626783), anti-NLRP3 (mouse, 1:300, AdipoGen Life Sciences, San Francisco, CA, USA, Cat# AG-20B-0014, RRID: AB_2490202), anti-IL18 (rabbit, 1:200, Santa Cruz Biotechnology, Cat# sc-7954, RRID: AB_1564060), anti-IL-1β (mouse, 1:500, Santa Cruz Biotechnology, Cat# sc-32294, RRID: AB_627790), anti-cleaved caspase-1 (rabbit, 1:250, Santa Cruz Biotechnology, Cat# sc-514, RRID: AB_2068895), anti-cleaved caspase-3 (rabbit, 1:1000, Cell Signaling Technology, Danvers, MA, USA, Cat# 9664, RRID: AB_2070042), anti-GAPDH (mouse, 1:10,000, Millipore, Burlington, MA, USA, Cat# MAB374, RRID: AB_2107445). All the primary antibodies were incubated overnight at 4°C. Following washing, HRP-conjugated secondary antibodies were added to the membranes, mouse HRP-conjugated (mouse, 1:5000, Merck, Cat# A9044) and rabbit HRP-conjugated (rabbit, 1:8000, Merck, Cat# A9169). The ECL system (ECL Plus; Thermo Fisher Scientific, Waltham, MA, USA) was used to develop the membranes. The ImageJ 1.44p software (NIH, Bethesda, MD, USA; Schneider et al., 2012) analysis program was used to quantify the band intensity. The densitometric analysis is shown in arbitrary units normalized to GAPDH as the loading control. The cell

lysate from the astrocyte primary cell culture was obtained as previously described (Mellado et al., 2023) and used as the positive control for calnexin, and as the negative control for CD9, CD63, and CD81.

RNA isolation, reverse transcription and quantitative PCR

Total RNA extraction was performed on the frozen hippocampal samples. The total RNA fraction was extracted in accordance with the manufacturer's instructions after the tissues were disrupted using TRIzol (Sigma). The NZY First-Strand cDNA Synthesis Kit (NZYTech, Lda., Lisboa, Portugal) and TaqMan™ Advanced miRNA Assays (Thermo Fisher Scientific) were utilized for the reverse transcription of total mRNA and total miRNA, respectively.

A QuantStudio™ 5 Real-Time PCR System (Applied Biosystems, Woburn, MA, USA) was used to conduct RT-qPCR. Using the AceQ ® qPCR SYBR Green Master Mix (NeoBiotech, Nanterre, France) and according to the manufacturer's instructions, genes were amplified. Internal control for the normalization of the examined genes was the mRNA level of the housekeeping gene cyclophilin A. Thermo Fisher Scientific's TaqMan™ Fast Advanced Master Mix was utilized to amplify specific miRNAs, and snRNA U6 served as an internal control. The ΔΔCq method was used to quantify the expression (fold change) from the Cq data (Schmittgen and Livak, 2008) by the QuanStudio™ Design & Analysis Software (Applied Biosystems). The information on the nucleotide sequences of the primers used and the miRNA assays is shown in **Additional Tables 1** and **2**.

Bioinformatic analysis of miRNAs

Based on the three miRNAs of interest (mmu-miR-21a-5p, mmu-miR-141-5p, mmu-miR-146a-5p), we used the multiMiR package and database (version 1.16.0; http://multimir.org/; Ru et al., 2014) to obtain their validated target genes. Subsequently, we conducted an overrepresentation analysis using the ClusterProfiler package (version 4.2.2; https://bioconductor.org/; Wu et al., 2021) to identify the KEGG (Kyoto Encyclopedia of Genes and Genomes) pathways (Kanehisa and Goto, 2000) that are enriched in the list of target genes, compared with what would be expected by chance. We then compared the results for each miRNA to evaluate the similarities. The R version used for this analysis was 4.1.2 (R Core Team, 2021). Protein-protein interaction (PPI) networks were also constructed using the STRING web tool (https://string-db.org/) for the target-shared genes among the three miRNAs (Szklarczyk et al., 2023). The PPI enrichment was assessed using a minimum required interaction score of "high confidence" (0.7).

Statistical analysis

The results were expressed as the mean±SEM. Data analysis was performed via SPSS version 28 (IBM IBM Corp, Armonk, NY, USA). The Shapiro-Wilk normality test was used to test the normality of the variable distribution. For comparisons between multiple groups, a one-way analysis of variance with Bonferroni's *post hoc* test was performed. $P < 0.05$ values were regarded as statistically significant.

Results

Characterization of MSC-EVs

Using electron microscopy, tracking analysis of nanoparticles, and EV markers, we first characterized MSC-EVs (**Figure 1**). The size and shape of the particles derived from MSCs were found to exhibit typical exosome characteristics, as demonstrated by the transmission electron microscopy study. Nevertheless, these nanoparticles are named EVs, since it was uncertain whether all the nanoparticles were exosomes (diameter of approximately 100 nm; **Figure 1A**). Moreover, the tetraspanin proteins (CD63, CD9, and CD81), which were exosome markers, were expressed by these EVs, and they showed no indications of cytosolic protein contamination, as evidenced by the absence of calnexin protein (**Figure 1B**). Using NanoSight, we further examined the size distribution and concentration of the nanoparticles secreted by MSCs. The findings showed that the range of 100–200 nm, which corresponds to the size range of EVs, was where the highest peak of the secreted nanoparticles fell (**Figure 1C**).

MSC-EVs alleviate the activation of the NLRP3 inflammasome pathway in the hippocampus of adolescent mice treated with binge-like ethanol treatment

Our previous results demonstrated that MSC-EVs from adipose tissue were able to ameliorate the neuroinflammation induced by binge drinking in adolescent mice (Mellado et al., 2023). Considering that ethanol can activate the NLRP3 inflammasome in astroglial cells and the cerebral cortices of mice (Alfonso-Loeches et al., 2014, 2016), we, therefore, wondered if an intravenous injection of MSC-EVs was also capable of decreasing the activation of the NLRP3 inflammasome pathway in the hippocampus of ethanol-treated adolescent mice. To answer this question, we first evaluated the components of the NLRP3 inflammasome complex, which requires the adaptor protein ASC and caspase-1 to activate cytokine release (Almeida-da-Silva et al., 2023). **Figure 2A** shows that the ethanol treatment significantly increased the gene expression of *NLRP3* [$F_{(3,28)}$ = 2.103, $P < 0.0001$], *caspase-1* ($F_{(3,27)}$ = 0.5897, $P < 0.0001$) and *ASC* ($F_{(3,27)}$ = 0.8906, $P = 0.0147$) compared with the saline-treated adolescents. Analyzing the cytokine expression, ethanol significantly increased the mRNA expression of *IL-1β* ($F_{(3,27)}$ = 4.358, $P = 0.0056$) and *IL-18* ($F_{(3,28)}$ = 2.534, $P = 0.0024$) compared with the saline group (**Figure 2B**). Notably, the administration of MSC-EVs significantly attenuated the ethanol-induced mRNA expression of the NLRP3 inflammasome complex (ethanol + EVs *vs*. ethanol) (*NLRP3* [$F_{(3,28)}$ = 2.103, $P = 0.0001$], *caspase-1* [$F_{(3,27)}$ = 0.5897, $P = 0.0005$] and *ACS* [$F_{(3,27)}$ = 0.8906, $P = 0.0025$]; **Figure 2A**) and the cytokine expression of *IL-1β* ($F_{(3,27)}$ = 4.358, $P < 0.0001$), and *IL-18* ($F_{(3,28)}$ = 2.534, $P = 0.0023$; **Figure 2B**). These data also showed a significant increase in animals treated with ethanol in comparison to animals treated with saline + MSC-EVs in the gene expression of *NLRP3* ($F_{(3,28)}$ = 2.103, $P < 0.0001$), *caspase-1* ($F_{(3,27)}$ = 0.5897, $P = 0.0001$), *ACS* ($F_{(3,27)}$ = 0.8906, $P < 0.0207$), *IL-1β* ($F_{(3,27)}$ = 4.358, $P = 0.0014$), and *IL-18* ($F_{(3,28)}$ = 2.534, $P < 0.0001$).

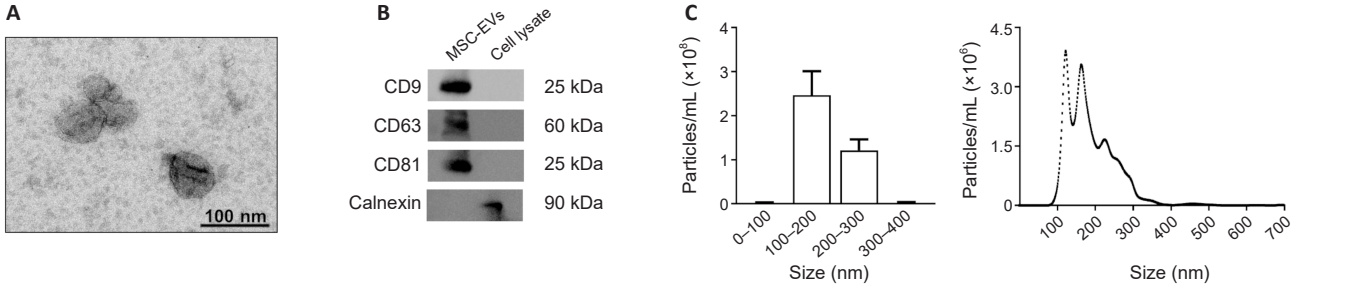

Figure 1 | **Characterization of MSC-EVs.**
(A) Electron microscopy image of MSC-EVs. (B) Analysis of the protein expression of EV markers (CD9, CD63, and CD81) in EVs and cell lysates. Calnexin expression was used to discount cytosolic protein contamination in EV samples. Cell lysates from astroglial cells were used as a positive control for calnexin expression. A representative immunoblot for each protein is shown. (C) Measurement of the size distribution and concentration of MSC-EVs by the nanoparticles tracking analysis. A high peak ranging between 100 and 200 nm is shown, which includes the size range of EVs. EVs: Extracellular vesicles; MSC-EVs: mesenchymal stem cell-derived EVs.

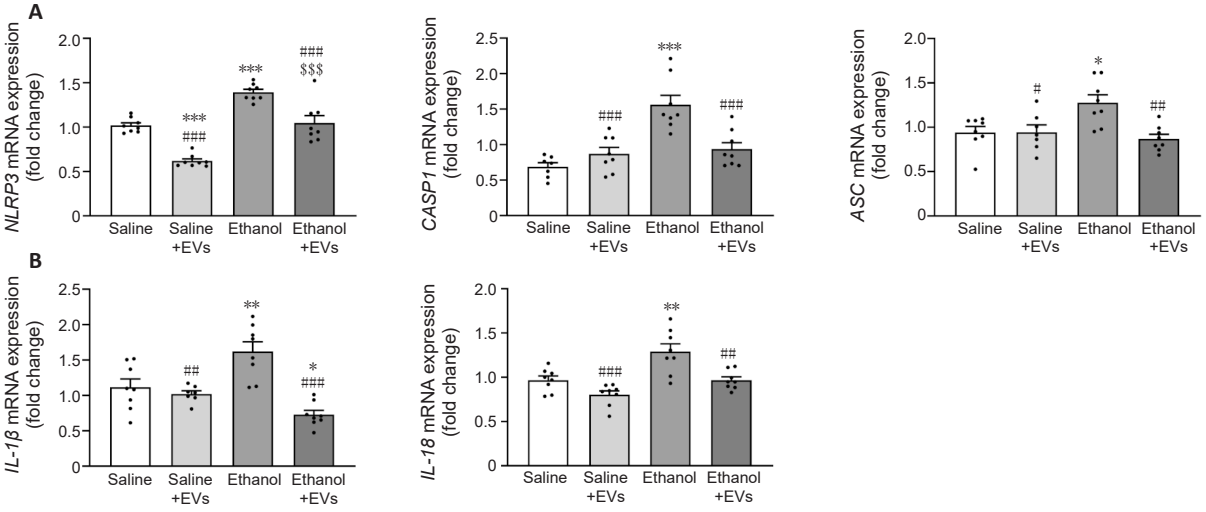

Figure 2 | **MSC-EVs attenuate the activation of hippocampal NLRP3 inflammasome complex induced by binge-like ethanol treatment in adolescent mice.**
(A) The mRNA expression of components of the NLRP3 inflammasome complex, such as *NLRP3*, *CASP-1*, and *ASC* in the hippocampus. (B) The mRNA expression of the proinflammatory *IL-1β* and *IL-18*. Data are presented as mean ± SEM, $n = 8$ mice/group. *$P < 0.05$, **$P < 0.01$, ***$P < 0.001$, *vs.* saline-treated group; #$P < 0.05$, ##$P < 0.01$, ###$P < 0.001$, *vs.* ethanol-treated group; $$$$P < 0.001$, *vs.* saline + MSC-EVs treated group (one-way analysis of variance with Bonferroni's *post hoc* test). ASC: Apoptosis-associated speck-like protein containing a CARD; CASP-1: caspase-1; EVs: extracellular vesicles; IL: interleukin; mRNA: messenger ribonucleic acid; MSC-EVs: mesenchymal stem cell-derived EVs; NLRP3: NOD-, LRR- and pyrin domain-containing protein 3.

We then analyzed whether an intravenous injection of MSC-EVs could also reduce the activation of the NLRP3 inflammasome pathway in the hippocampus of ethanol-treated adolescent mice at the protein level. Ethanol treatment significantly increased the protein expression of NLRP3 ($F_{(3,16)} = 0.2037$, $P = 0.0002$), IL-1β ($F_{(3,17)} = 0.5356$, $P = 0.0358$), IL-18 ($F_{(3,16)} = 0.2529$, $P = 0.0198$), cleaved caspase-1 ($F_{(3,16)} = 0.8246$, $P = 0.0003$) and cleaved caspase-3 ($F_{(3,16)} = 2.769$, $P < 0.0001$) compared with the saline-treated adolescents (**Figure 3**). Indeed, the activation of both caspases in ethanol-treated animals was evidenced by the increase in active caspase-1 (10 kDa) and caspase-3 (17 kDa) peptides. Notably, the administration of MSC-EVs significantly attenuated the upregulation in these proteins in ethanol-treated animals (ethanol + EVs *vs*. ethanol) (NLRP3 [$F_{(3,16)} = 0.2037$, $P = 0.0126$], IL-1β [$F_{(3,17)} = 0.5356$, $P = 0.0300$], IL-18 [$F_{(3,16)} = 0.2529$, $P = 0.0066$], cleaved caspase-1 [$F_{(3,16)} = 0.8246$, $P < 0.0001$] and cleaved caspase-3 [$F_{(3,16)} = 2.769$, $P < 0.0001$]; **Figure 3**).

Considering that several inflammatory molecules, such as caspase-11/4, TLR4 or IRAK1 may activate the NLRP3/caspase-1 complex (Kelley et al., 2019; Zheng et al., 2020), we then evaluated the gene expression of these genes (**Figure 4A**). The results showed that while ethanol treatment increased the levels of *caspase-11/4* ($F_{(3,27)} = 0.3200$, $P < 0.0001$), *TLR4* ($F_{(3,28)} = 0.3609$, $P = 0.0181$) and *IRAK1* ($F_{(3,28)} = 1.592$, $P = 0.0438$), the administration of MSC-EVs significantly restored the upregulation I of these genes (*caspase-11/4* [$F_{(3,27)} = 0.3200$, $P < 0.0001$], *TLR4* ($F_{(3,28)} = 0.3609$, $P = 0.0122$) and *IRAK1* ($F_{(3,28)} = 1.592$, $P = 0.0446$) in ethanol-treated mice. A significant increase was also shown in mice treated with ethanol compared with animals treated with saline + MSC-EVs (*caspase-11/4* [$F_{(3,27)} = 0.3200$, $P < 0.0001$], *TLR4* [$F_{(3,28)} = 0.3609$, $P = 0.0003$] and *IRAK1* [$F_{(3,28)} = 1.592$, $P < 0.0009$]).

To delve deeper into whether other NLRs were activated in the hippocampus of ethanol-treated adolescent mice, the gene expression of *NLRP1*, *NLRC4*, and *AIM2* was also assessed. Whereas ethanol treatment significantly upregulated the expression of *NLRP1* ($F_{(3,28)} = 0.6065$, $P =$

0.0023), *AIM2* ($F_{(3,28)}$ = 0.4111, *P* = 0.0119) and *NLRC4* ($F_{(3,28)}$ = 3.775, *P* = 0.0027), the intravenous injection of MSC-EVs significantly attenuated these increases in ethanol-treated adolescent mice (*NLRP1* [$F_{(3,28)}$ = 0.6065, *P* = 0.0209], *AIM2* [$F_{(3,28)}$ = 0.4111, *P* = 0.0472] and *NLRC4* [$F_{(3,28)}$ = 3.775, *P* = 0.0407]; **Figure 4B**). We noted a significant increase in animals treated with ethanol in comparison with animals treated with saline + MSC-EVs (*NLRP1* [$F_{(3,28)}$ = 0.6065, *P* = 0.0021], *AIM2* [$F_{(3,28)}$ = 0.4111, *P* = 0.0072] and *NLRC4* [$F_{(3,28)}$ = 3.775, *P* = 0.0024]; **Figure 4B**).

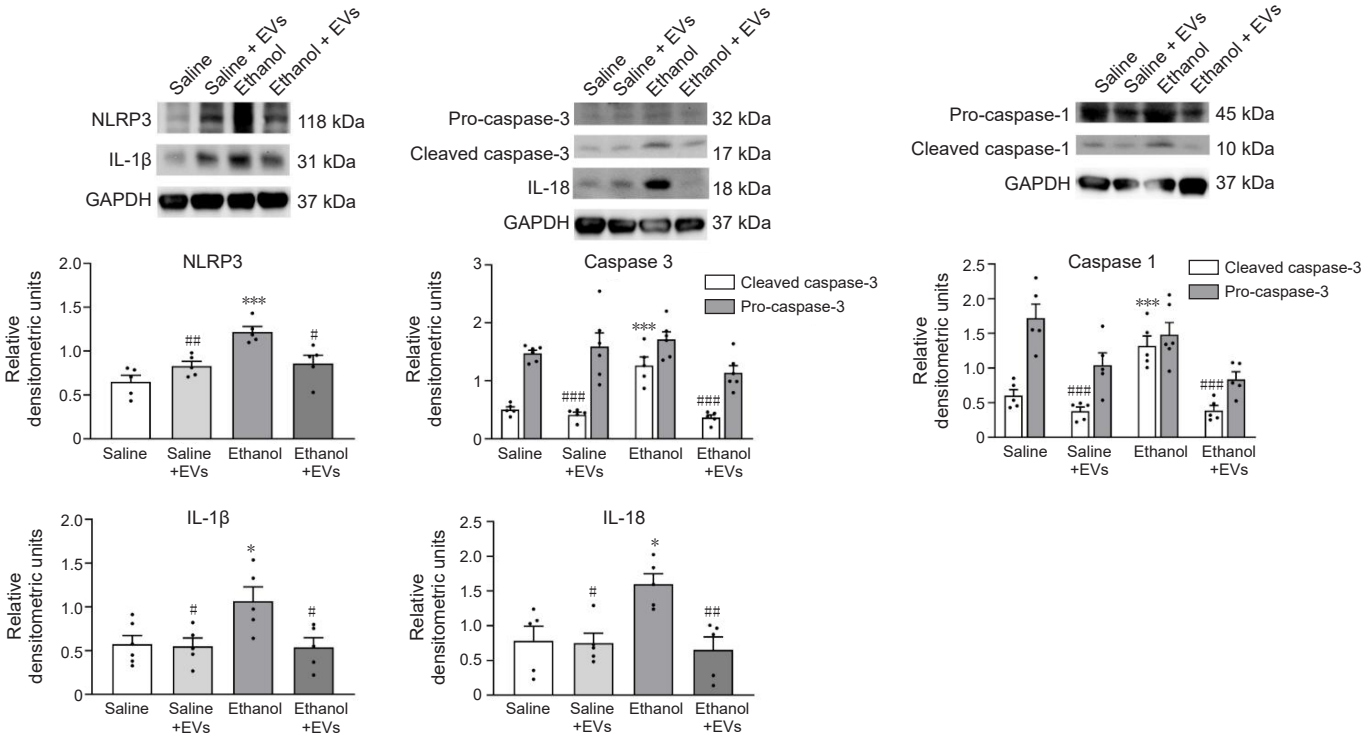

Figure 3 | **MSC-EVs ameliorate the expression of some NLRP3 inflammasome proteins induced by binge-like ethanol treatment in adolescent mice.**
The protein expression of NLRP3, the cleaved- and pro-caspase-1, the cleaved- and pro-caspase-3, and the proinflammatory cytokines, IL-1β and IL-18 in the hippocampus. Data represent mean±SEM, *n* = 6 mice/group. **P* < 0.05, ****P* < 0.001, *vs*. saline-treated group; #*P* < 0.05, ##*P* < 0.01, ###*P* < 0.001, *vs.* ethanol-treated group (one-way analysis of variance with Bonferroni's *post hoc* test). EVs: Extracellular vesicles; IL: interleukin; MSC-EVs: mesenchymal stem cell-derived EVs; NLRP3: NOD-, LRR- and pyrin domain-containing protein 3.

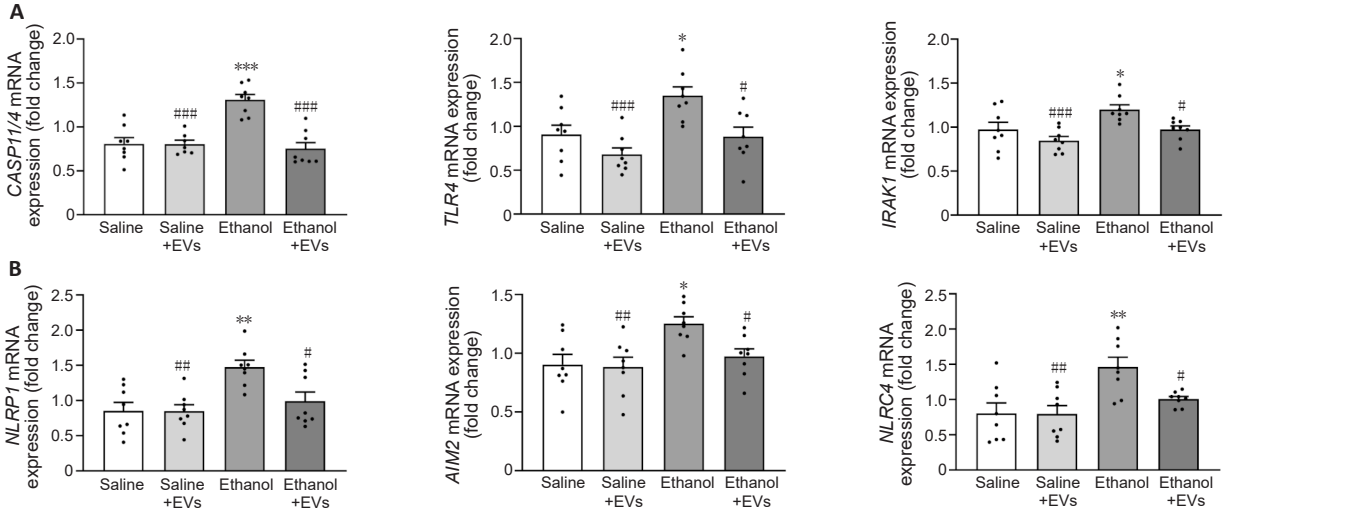

Figure 4 | **MSC-EVs diminish the activation of other NLR-related genes induced by binge-like ethanol treatment in adolescent mice.**
(A) The mRNA expression of *CASP11/4*, *TLR4*, and *IRAK1* in the hippocampus. (B) The mRNA expression of *NLRP1*, *AIM2* and *NLRC4*. Data are presented as mean±SEM, *n* = 8 mice/group. **P* < 0.05, ***P* < 0.01, ****P* < 0.001, *vs.* saline-treated group; #*P* < 0.05, ##*P* < 0.01, ###*P* < 0.001, *vs*. ethanol-treated group (one-way analysis of variance with Bonferroni's *post hoc* test). AIM2: Absent in melanoma 2; CASP11/4: caspase-11/14; EVs: extracellular vesicles; IL: interleukin; IRAK: interleukin 1 receptor associated kinase 1; MSC-EVs: mesenchymal stem cell-derived EVs; NLRP1: pyrin domain-containing 1; NLRC4: caspase recruitment domain-containing 4; NLRP3: NOD-, LRR- and pyrin domain-containing protein 3; NLRs: nucleotide-binding oligomerization domain-like receptors; TLR4: toll-like receptor 4.

MSC-EVs ameliorate hippocampal inflammatory genes and miRNAs induced by binge-like ethanol treatment in adolescent mice

We then examined whether the administration of MSC-EVs could reverse the ethanol-induced up-regulation of inflammatory gene mRNA levels. We measured the hippocampal inducible nitric oxide synthase (iNOS), nuclear factor-kappa B (NF-κB), monocyte chemoattractant protein-1 (MCP-1), and C–X3–C motif chemokine ligand 1 (CX3CL1) levels under various experimental setups. Ethanol treatment significantly increased *iNOS* ($F_{(3,28)}$ = 1.481, P = 0.0051), *NF-κB* ($F_{(3,28)}$ = 0.09025, P = 0.0116), *MCP-1* ($F_{(3,28)}$ = 3.211, P = 0.0145), and *CX3CL1* ($F_{(3,28)}$ = 1.159, P = 0.0019) gene expression compared with their saline counterparts (**Figure 5**). As expected, compared with the mice treated with ethanol, the administration of MSC-EVs significantly reduced the ethanol-induced expression of these proinflammatory molecules (*iNOS* [$F_{(3,28)}$ = 1.481, P = 0.0411], *NF-κB* [$F_{(3,28)}$ = 0.09025, P = 0.0195], *MCP-1* [$F_{(3,28)}$ = 3.211, P = 0.0010], and *CX3CL1* [$F_{(3,28)}$ = 1.159, P = 0.0002]). In addition, ethanol treatment significantly increased *iNOS* ($F_{(3,28)}$ = 1.481, P = 0.0013), *NF-κB* ($F_{(3,28)}$ = 0.09025, P = 0.0006), *MCP-1* ($F_{(3,28)}$ = 3.211, P = 0.0007), and *CX3CL1* ($F_{(3,28)}$ = 1.159, P < 0.0001) levels compared with the mice treated with saline plus MSC-EVs (**Figure 5**). There were no differences in the expression of these genes between the animals treated with saline and MSC-EVs.

We then explored whether the alterations observed in the expression of the inflammatory genes (**Figures 2**, **4**, and **5**) in the hippocampus of ethanol-treated adolescent mice could be associated with the changes in the expression of several miRNAs, such as *miR-21a-5p*, *miR-141-5p* and *miR-146a-5p* (**Figure 6**). In fact, we have demonstrated that treatment with ethanol modifies the expression of particular miRNAs linked to neuroinflammation (e.g., *miR-183* cluster, *miR-200*, *miR-141-5p*, and *miR-146a-5p*) in mouse cerebral cortices (Ureña-Peralta et al., 2018; Ibáñez et al., 2020) and in astrocyte cell cultures (Ibáñez et al., 2019). Notably, a significant increase in the *miR-21a-5p* ($F_{(3,27)}$ = 3.749, P = 0.0001), *miR-141-5p* ($F_{(3,27)}$ = 1.424, P = 0.0398) and *miR-146a-5p* ($F_{(3,26)}$ = 3.522, P < 0.01) levels were found in the ethanol-treated animals. These expressions significantly decreased in the adolescent mice treated with ethanol plus MSC-EVs compared with the ethanol-treated animals (*miR-21a-5p* [$F_{(3,27)}$ = 3.749, p < 0.0001], *miR-141-5p* [$F_{(3,27)}$ = 1.424, P = 0.0008] and *miR-146a-5p* [$F_{(3,26)}$ = 3.522, P = 0.0002]). Saline plus MSC-EVs-treated mice showed significantly lower levels of expression compared with the ethanol-treated group (*miR-21a-5p* [$F_{(3,27)}$ = 3.749, P < 0.0001], *miR-141-5p* [$F_{(3,27)}$ = 1.424, P = 0.0006] and *miR-146a-5p* [$F_{(3,26)}$ = 3.522, P = 0.0002]).

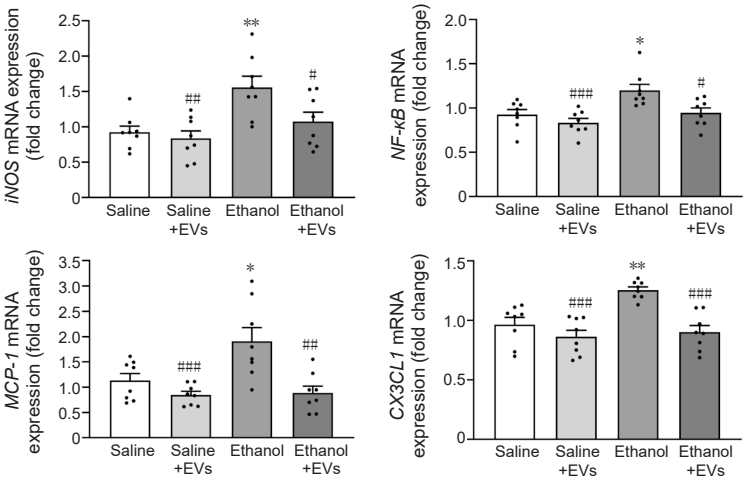

Figure 5 | MSC-EVs decrease the levels of inflammatory genes induced by binge-like ethanol treatment in adolescent mice.

The mRNA expression of *iNOS*, *NF-κB*, *MCP-1*, and *CX3CL1* were analyzed in the hippocampal samples. Data are presented as mean±SEM, n = 8 mice/group. *P < 0.05, **P < 0.01, *vs*. saline-treated group; #P < 0.05, ##P < 0.01, ###P < 0.001, *vs*. ethanol-treated group (one-way analysis of variance with Bonferroni's *post hoc* test). CX3CL1: C–X3–C motif chemokine ligand 1; EVs: extracellular vesicles; iNOS: inducible nitric oxide synthase; MCP-1: monocyte chemoattractant protein-1; MSC-EVs: mesenchymal stem cell–derived EVs; NF-κB: nuclear factor-kappa B.

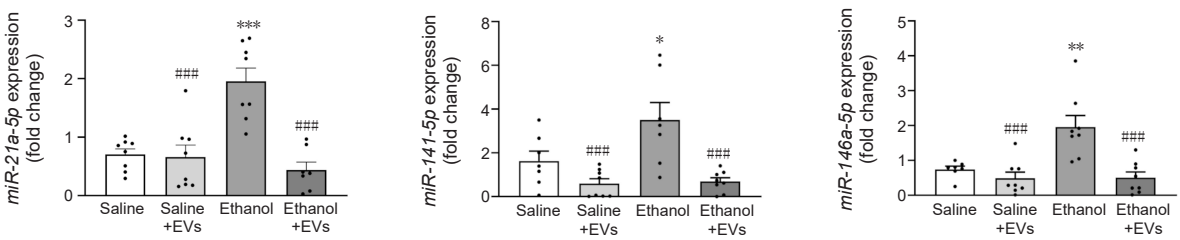

Figure 6 | MSC-EVs restore the levels of *miR-21a-5p*, *miR-141-5p* and *miR-146a-5p* in the hippocampus of binge-like ethanol-treated adolescent mice.

Data are presented as mean±SEM, n = 8 mice/group. *P < 0.05, **P < 0.01, ***P < 0.001, *vs.* saline-treated group; ###P < 0.001, *vs.* ethanol-treated group (one-way analysis of variance with Bonferroni's *post hoc* test). EVs: Extracellular vesicles; miR: microRNA; MSC-EVs: mesenchymal stem cell-derived EVs.

Bioinformatic analysis results of miRNAs involved in the effects of ethanol and MSC-EVs

After confirming that MSC-EVs were able to reverse the ethanol-induced alterations in the levels of some miRNAs (*miR-21a-5p*, *miR-146a-5p*, and *miR-141-5p*), we conducted a functional analysis of these miRNAs to establish the key pathways and biological functions involved in the effects of ethanol and MSC-EVs. First, we determined the main targets modulated by these. The analysis demonstrated that the 2205, 397 and 4 target genes were modulated by *miR-21a-5p*, *miR-146a-5p*, and *miR-141-5p*, respectively (data not shown). **Figure 7A** reveals that *miR-21a-5p* and *miR-146a-5p* displayed a stronger interaction with the modulated target genes than the other two intersections, which had 0 or 1 shared genes. For instance, *miR-21a-5p* and *mir-146a-5p* control immune target genes, such as *Irak2*, *Ccr5*, *Cxcr4*, *Irf4*, *Tirap*, *Cd28*, and *Camk2d*, as well as a gene required for RNA-mediated gene expression named Ago2. Using the STRING web tool, we created PPI networks for the 119 miRNA-targeted shared genes (**Figure 7A**). Within the PPI analysis, we obtained three larger clusters and six with almost one connection (**Figure 7B**). The results revealed more significant interactions in the network than anticipated (PPI enrichment *P*-value: 9.09e-6), suggesting there were more connections among these proteins than would be expected in a random collection of proteins with similar sizes and degree distributions taken from the genome. This enrichment indicates that these proteins shared at least some biological relationships with each other. Afterwards, we conducted an overrepresentation analysis using the KEGG pathways, which allowed us to identify the signaling pathways enriched in the list of all the target genes. **Figure 7C** showed the significantly enriched KEGG pathways obtained by miRNA and the number of miRNA-regulated genes that participated in the significantly enriched KEGG pathways for each miRNA. Although the three miRNAs were able to modulate signaling pathways associated with the immune response and inflammatory processes (e.g., TLR, cytokine receptor, chemokine, B cell receptor TGF-β, and MAPK), the *miR-21a-5p* was able to modify the NOD-like receptor signaling pathway.

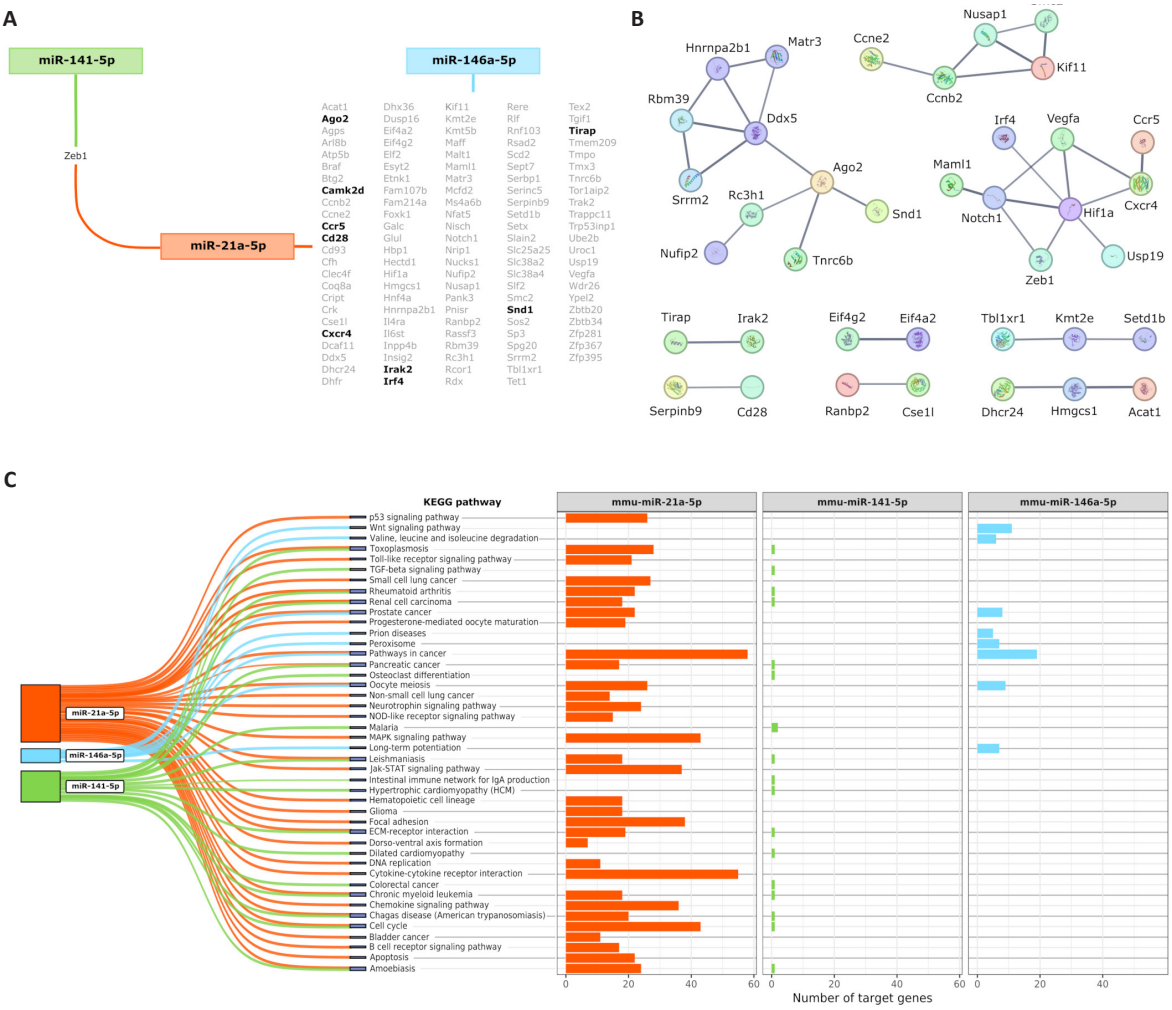

Figure 7 | **The main results of bioinformatics analysis focused on the miRNAs *miR-21a-5p*, *miR-141-5p*, and *miR-146a-5p*.**
(A) Target genes shared by the miRNAs. Genes highlighted in black are related to processes involved in the immune response and RNA-mediated gene expression. (B) PPI networks generated from all the miRNA-targeted shared genes. Line thickness indicates the strength of data support. (C) Number of miRNA-targeted genes that participate in the significantly enriched KEGG pathways for each miRNA. KEGG: Kyoto Encyclopedia of Genes and Genomes; miR: microRNA; PPI: protein–protein interaction.

Discussion

We have recently shown that MSC-EVs have a therapeutic role in restoring neuroinflammation, myelin, and synaptic structural changes in the prefrontal cortex, along with cognitive dysfunctions induced by binge-like ethanol treatment in adolescent mice (Mellado et al., 2023). Considering the involvement of the inflammasome receptors in the neuroinflammatory processes (Piancone et al., 2021) and behavioral dysfunctions (Jin et al., 2019; Hou et al., 2020), the present findings provide evidence that the intravenous administration of MSC-EVs restores the activation of the NLRP3 inflammasome complex and other NLRs inflammasomes (e.g., NLRP1, NLRC4, and AIM2), as well as the alterations of inflammatory genes and miRNAs in the hippocampus induced by binge-like ethanol treatment in adolescent mice (**Figure 8**).

Our previous studies revealed the role of NLRP3/caspase-1 complex activation, along with the up-regulated pro-inflammatory cytokines and chemokines levels in ethanol-treated astrocytes and in cortices from chronic alcohol-fed WT mice (Alfonso-Loeches et al., 2014, 2016). Likewise, we have also provided evidence that binge-ethanol treatment in adolescent mice activates NLRs and their signaling pathways, inducing a neuroinflammatory response. Since the MSC-EVs from adipose tissue were capable of diminishing the prefrontal cortex neuroinflammation induced by binge drinking in adolescent mice (Mellado et al., 2023), the use of these microvesicles could also participate in ameliorating the inflammasome complex in the hippocampus. In this line, it has been reported that the administration of MSC-EVs alleviates the inflammatory response by inhibiting the activation of NLRP3 inflammasome in an Alzheimer's disease mouse model (Xu et al., 2022), in spinal cord injury (Noori et al., 2021), or in lipopolysaccharide-induced cardiomyocyte inflammation (Pan et al., 2022). The present study provides evidence that MSC-EVs restore the activation, not only of the hippocampal NLRP3 inflammasome complex, but also of up-regulated inflammatory genes (*IL-1β*, *IL-18*, *iNOS*, *NF-κB*, *MCP-1*, and *CX3CL1*) and miRNAs (*miR-21a-5p*, *miR-141-5p*, and *miR-146a-5p*) in the hippocampus of adolescent mice with binge-like ethanol treatment. Indeed, the bioinformatic analysis of *miR-21a-5p* and *miR-146a-5p* revealed the involvement of these miRNAs with inflammatory target genes and NOD-like receptor signaling pathways.

In recent years, a large number of studies have reported the therapeutic effects of miRNAs contained within MSC-EVs (Harrell et al., 2019; Mathew et al., 2023; Vaka et al., 2023). These therapeutic effects have been attributed to their actions in regulating the expression of multiple target genes and in modulating various cell signaling processes to promote functional recovery (Qiu et al., 2018). Patients with neurodegenerative diseases have been shown to exhibit dysregulation of circulating levels of particular EV-miRNAs. Several EV-miRNAs (e.g., *miR-124a*, *miR-146a*, *miR-21*, *miR-29b*, and *miR-873a-5p*) have been reported to show potential effects to reduce oxidative stress and neuroinflammation in Alzheimer's disease or traumatic brain injury models (Bang and Kim, 2022). Another study has also demonstrated the protective function of these microvesicles by transferring the *miR-223-3p* to suppress the circular RNA PWWP2A, thereby alleviating pulmonary fibrosis through the NLRP3 signaling pathway (Hou et al., 2023). Conversely, our results showed that MSC-EVs were able to diminish the levels of the inflammatory miRNAs (*miR-21a-5p*, *miR-146a-5p*, and *miR-141-5p*) induced by binge-like ethanol treatment in adolescent mice. Accordingly, a TLRs inflammatory response, associated with the upregulation of the *miR-132*, can be decreased through this miRNA located within MSC-EVs by increasing the IL-10 expression and decreasing NF-κB and IL-1β levels (Wang et al., 2020). Although miRNAs can modulate gene expression, additional molecules (e.g., Argonaute protein, Drosha, DGCR8, or NRSF) may regulate the transcription of these miRNA, either positively or negatively, modifying cell fate (Ergin and Çetinkaya, 2022). Therefore, we suggest that MSC-EVs could

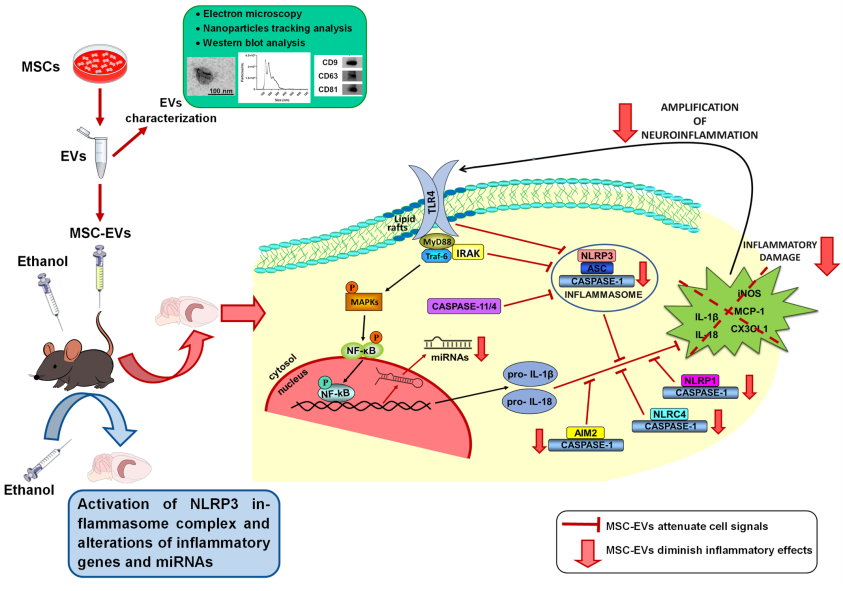

Figure 8 | Protective effects of MSC-EVs on ethanol-induced hippocampal neuroinflammation by inhibiting NLRP3 inflammasome activation.
MSC-EVs were isolated from adipose tissue, and then EVs were characterized by electron microscopy, nanoparticle tracking analysis, and Western blotting. MSC-EVs were administered by intravenous injection (iv) prior to ethanol treatment (intraperitoneal injection, ip) in adolescent mice. MSC-EVs administration ameliorates the activation of the hippocampal NLRP3 inflammasome complex and other NLRs inflammasomes (e.g., NLRP1, NLRC4, and AIM2), as well as the alterations in the expression of inflammatory genes and miRNAs induced by binge-like ethanol treatment in adolescent mice. AIM2: Absent in melanoma 2; EVs: extracellular vesicles; IL: interleukin; MSC-EVs: mesenchymal stem cell-derived EVs; NLRC4: caspase recruitment domain-containing 4; NLRP1: pyrin domain-containing 1; NLRP3: NOD-, LRR- and pyrin domain-containing protein 3; NLRs: nucleotide-binding oligomerization domain-like receptors; TLR4: toll-like receptor 4

transfer their content to neural cells, activating silencing transcription factors or enzymes, which could prevent the transcription of inflammatory miRNAs (*miR-21a-5p*, *miR-146a-5p*, and *miR-141-5p*), thereby promoting functional recovery in ethanol-treated adolescent mice.

The hippocampus is an important brain area associated with memory and learning processes (Gandhi et al., 2014; Pascual et al., 2021). Therefore, the involvement of the MSC-EVs in restoring the alterations in the NLPR3 inflammasome induced by binge-like ethanol treatment in the adolescent hippocampus could also contribute to the ethanol-induced cognitive dysfunction shown in a study by Mellado et al. (2023). Several studies have reported that spatial memory dysfunction could be related to the neuroinflammation induced by the hippocampal activation of the NLRP3 inflammasome and the TLR4/NF-κB signaling pathway in a mouse model of Alzheimer's disease (Jin et al., 2019) and in an experimental autoimmune encephalomyelitis (Hou et al., 2020). Additionally, these cognitive impairments could also be associated with the activation of different caspases, leading to brain damage and neurodegeneration (Glushakova et al., 2017; Cheon et al., 2020). Our results showed that MSC-EVs restore the activation of the apoptotic caspase-3 and the inflammatory caspase-1 in the hippocampus of ethanol-treated adolescent mice, suggesting that MSC-EVs may be associated with inhibiting hippocampal neuroinflammation and neurodegeneration by suppressing the activation of both caspases in binge ethanol drinking.

Our interest in this study was to provide the therapeutic role of MSC-EVs from adipose tissue in restoring the NLPR3 neuroinflammatory response induced by binge drinking in adolescence. While adipose tissue is easily accessible and abundant, making it one of the most favorable options for obtaining MSCs, this study also presents some limitations. For instance, 1) we used the term EVs since we cannot distinguish between exosomes and microvesicles, which have similar size and protein markers, 2) the miRNA profile of MSC-EV varies depending on the origin tissue, and 3) we cannot discard the possibility of other miRNAs or molecules being involved in the neuroprotective effects. In this sense, future studies could be aimed to demonstrate if the MSCs from other tissues, such as bone marrow, peripheral blood, cord blood, or fetal tissues, could also ameliorate the NLRP3 neuroinflammatory response induced by binge drinking in adolescence.

All of these findings provide evidence of the protective function of MSC-EVs in the hippocampal neuroinflammatory immune response by activating the NLRP3 inflammasome complex induced by binge-like ethanol treatment during adolescence. This study also sheds light on a potential mechanism of action in the effects of ethanol and MSC-EVs in the inflammasome alterations through the regulation of *miR-21a-5p* and *mir-146a-5p*. In conclusion, the present findings suggest the therapeutic potential of MSC-EVs as a new tool to restore the neuroinflammatory response related to alcohol consumption and brain damage.

Author contributions: *MP, SM, and CG conceived and designed the experiments. SM, MJMB, and CPC performed the experiments and analyzed the data. SM, MJMB, CPC, CG, and MP wrote the manuscript. SM, FGG, VMM, CG, and MP revised the manuscript. All authors read and approved the final manuscript.*

Conflicts of interest: *The authors have no conflicts of interest to declare.*

Data availability statement: *All relevant data are within the paper and its Additional files.*

Additional files:

Additional Table 1: *Primer sequences of the analyzed genes used for quantitative PCR.*

Additional Table 2: *Nucleotide sequences of the primers used for quantitative PCR of microRNAs.*

References

Alfonso-Loeches S, Ureña-Peralta JR, Morillo-Bargues MJ, Oliver-De La Cruz J, Guerri C (2014) Role of mitochondria ROS generation in ethanol-induced NLRP3 inflammasome activation and cell death in astroglial cells. Front Cell Neurosci 8:216.

Alfonso-Loeches S, Ureña-Peralta J, Morillo-Bargues MJ, Gómez-Pinedo U, Guerri C (2016) Ethanol-induced TLR4/NLRP3 neuroinflammatory response in microglial cells promotes leukocyte infiltration across the BBB. Neurochem Res 41:193-209.

Allen-Worthington KH, Brice AK, Marx JO, Hankenson FC (2015) Intraperitoneal injection of ethanol for the euthanasia of laboratory mice (Mus musculus) and rats (Rattus norvegicus). J Am Assoc Lab Anim Sci 54:769-778.

Almeida-da-Silva CLC, Savio LEB, Coutinho-Silva R, Ojcius DM (2023) The role of NOD-like receptors in innate immunity. Front Immunol 14:1122586.

Bang OY, Kim JE (2022) Stem cell-derived extracellular vesicle therapy for acute brain insults and neurodegenerative diseases. BMB Rep 55:20-29.

Brust V, Schindler PM, Lewejohann L (2015) Lifetime development of behavioural phenotype in the house mouse (Mus musculus). Front Zool 12:S17.

Cheon SY, Kim J, Kim SY, Kim EJ, Koo BN (2020) Inflammasome and cognitive symptoms in human diseases: biological evidence from experimental research. Int J Mol Sci 21:1103.

Ergin K, Çetinkaya R (2022) Regulation of microRNAs. Methods Mol Biol Clifton NJ 2257:1-32.

Gandhi RM, Kogan CS, Messier C, Macleod LS (2014) Visual-spatial learning impairments are associated with hippocampal PSD-95 protein dysregulation in a mouse model of fragile X syndrome. Neuroreport 25:255-261.

Glushakova OY, Glushakov AA, Wijesinghe DS, Valadka AB, Hayes RL, Glushakov AV (2017) Prospective clinical biomarkers of caspase-mediated apoptosis associated with neuronal and neurovascular damage following stroke and other severe brain injuries: Implications for chronic neurodegeneration. Brain Circ 3:87-108.

Guerri C, Pascual M (2019) Impact of neuroimmune activation induced by alcohol or drug abuse on adolescent brain development. Int J Dev Neurosci Off J Int Soc Dev Neurosci 77:89-98.

Harrell CR, Jovicic N, Djonov V, Arsenijevic N, Volarevic V (2019) Mesenchymal stem cell-derived exosomes and other extracellular vesicles as new remedies in the therapy of inflammatory diseases. Cells 8:1605.

Harris JA, et al. (2019) Hierarchical organization of cortical and thalamic connectivity. Nature 575:195-202.

Hou B, Zhang Y, Liang P, He Y, Peng B, Liu W, Han S, Yin J, He X (2020) Inhibition of the NLRP3-inflammasome prevents cognitive deficits in experimental autoimmune encephalomyelitis mice via the alteration of astrocyte phenotype. Cell Death Dis 11:377.

Hou L, Zhu Z, Jiang F, Zhao J, Jia Q, Jiang Q, Wang H, Xue W, Wang Y, Tian L (2023) Human umbilical cord mesenchymal stem cell-derived extracellular vesicles alleviated silica induced lung inflammation and fibrosis in mice via circPWWP2A/miR-223-3p/NLRP3 axis. Ecotoxicol Environ Saf 251:114537.

Ibáñez F, Montesinos J, Ureña-Peralta JR, Guerri C, Pascual M (2019) TLR4 participates in the transmission of ethanol-induced neuroinflammation via astrocyte-derived extracellular vesicles. J Neuroinflammation 16:136.

Ibáñez F, Ureña-Peralta JR, Costa-Alba P, Torres JL, Laso FJ, Marcos M, Guerri C, Pascual M (2020) Circulating MicroRNAs in extracellular vesicles as potential biomarkers of alcohol-induced neuroinflammation in adolescence: gender differences. Int J Mol Sci 21:6730.

Jaszczyk A, Stankiewicz AM, Juszczak GR (2022) Dissection of mouse hippocampus with its dorsal, intermediate and ventral subdivisions combined with molecular validation. Brain Sci 12:799.

Jin X, Liu MY, Zhang DF, Zhong X, Du K, Qian P, Yao WF, Gao H, Wei MJ (2019) Baicalin mitigates cognitive impairment and protects neurons from microglia-mediated neuroinflammation via suppressing NLRP3 inflammasomes and TLR4/NF-κB signaling pathway. CNS Neurosci Ther 25:575-590.

Kanehisa M, Goto S (2000) KEGG: kyoto encyclopedia of genes and genomes. Nucleic Acids Res 28:27-30.

Kelley N, Jeltema D, Duan Y, He Y (2019) The NLRP3 inflammasome: an overview of mechanisms of activation and regulation. Int J Mol Sci 20:3328.

Le Merre P, Ährlund-Richter S, Carlén M (2021) The mouse prefrontal cortex: Unity in diversity. Neuron 109:1925-1944.

Mathew B, Acha LG, Torres LA, Huang CC, Liu A, Kalinin S, Leung K, Dai Y, Feinstein DL, Ravindran S, Roth S (2023) MicroRNA-based engineering of mesenchymal stem cell extracellular vesicles for treatment of retinal ischemic disorders: Engineered extracellular vesiclesand retinal ischemia. Acta Biomater 158:782-797.

Mellado S, Cuesta CM, Montagud S, Rodríguez-Arias M, Moreno-Manzano V, Guerri C, Pascual M (2023) Therapeutic role of mesenchymal stem cell-derived extracellular vesicles in neuroinflammation and cognitive dysfunctions induced by binge-like ethanol treatment in adolescent mice. CNS Neurosci Ther 29:4018-4031.

Mellado-López M, Griffeth RJ, Meseguer-Ripolles J, Cugat R, García M, Moreno-Manzano V (2017) Plasma rich in growth factors induces cell proliferation, migration, differentiation, and cell survival of adipose-derived stem cells. Stem Cells Int 2017:5946527.

Mira RG, Lira M, Tapia-Rojas C, Rebolledo DL, Quintanilla RA, Cerpa W (2019) Effect of alcohol on hippocampal-dependent plasticity and behavior: role of glutamatergic synaptic transmission. Front Behav Neurosci 13:288.

Montesinos J, Pascual M, Pla A, Maldonado C, Rodríguez-Arias M, Miñarro J, Guerri C (2015) TLR4 elimination prevents synaptic and myelin alterations and long-term cognitive dysfunctions in adolescent mice with intermittent ethanol treatment. Brain Behav Immun 45:233-244.

Montesinos J, Alfonso-Loeches S, Guerri C (2016) Impact of the innate immune response in the actions of ethanol on the central nervous system. Alcohol Clin Exp Res 40:2260-2270.

Muñoz-Criado I, Meseguer-Ripolles J, Mellado-López M, Alastrue-Agudo A, Griffeth RJ, Forteza-Vila J, Cugat R, García M, Moreno-Manzano V (2017) Human suprapatellar fat pad-derived mesenchymal stem cells induce chondrogenesis and cartilage repair in a model of severe osteoarthritis. Stem Cells Int 2017:4758930.

Noori L, Arabzadeh S, Mohamadi Y, Mojaverrostami S, Mokhtari T, Akbari M, Hassanzadeh G (2021) Intrathecal administration of the extracellular vesicles derived from human Wharton's jelly stem cells inhibit inflammation and attenuate the activity of inflammasome complexes after spinal cord injury in rats. Neurosci Res 170:87-98.

Pan L, Yan B, Zhang J, Zhao P, Jing Y, Yu J, Hui J, Lu Q (2022) Mesenchymal stem cells-derived extracellular vesicles-shuttled microRNA-223-3p suppress lipopolysaccharide-induced cardiac inflammation, pyroptosis, and dysfunction. Int Immunopharmacol 110:108910.

Pascual M, Blanco AM, Cauli O, Miñarro J, Guerri C (2007) Intermittent ethanol exposure induces inflammatory brain damage and causes long-term behavioural alterations in adolescent rats. Eur J Neurosci 25:541-550.

Pascual M, Montesinos J, Marcos M, Torres JL, Costa-Alba P, García-García F, Laso FJ, Guerri C (2017) Gender differences in the inflammatory cytokine and chemokine profiles induced by binge ethanol drinking in adolescence. Addict Biol 22:1829-1841.

Pascual M, López-Hidalgo R, Montagud-Romero S, Ureña-Peralta JR, Rodríguez-Arias M, Guerri C (2021) Role of mTOR-regulated autophagy in spine pruning defects and memory impairments induced by binge-like ethanol treatment in adolescent mice. Brain Pathol 31:174-188.

Piancone F, La Rosa F, Marventano I, Saresella M, Clerici M (2021) The role of the inflammasome in neurodegenerative diseases. Mol Basel Switz 26:953.

Qiu G, Zheng G, Ge M, Wang J, Huang R, Shu Q, Xu J (2018) Mesenchymal stem cell-derived extracellular vesicles affect disease outcomes via transfer of microRNAs. Stem Cell Res Ther 9:320.

Quigley J; Committee on Substance Use and Prevention (2019) Alcohol use by youth. Pediatrics 144:e20191356.

R Core Team (2021) R: A language and environment for statistical computing. R Foundation for Statistical Computing, Vienna, Austria. Available at: https://www.r-project.org/. Accessed August 2, 2023.

Ru Y, Kechris KJ, Tabakoff B, Hoffman P, Radcliffe RA, Bowler R, Mahaffey S, Rossi S, Calin GA, Bemis L, Theodorescu D (2014) The multiMiR R package and database: integration of microRNA-target interactions along with their disease and drug associations. Nucleic Acids Res 42:e133.

Schmittgen TD, Livak KJ (2008) Analyzing real-time PCR data by the comparative C(T) method. Nat Protoc 3:1101-1108.

Schneider CA, Rasband WS, Eliceiri KW (2012) NIH Image to ImageJ: 25 years of image analysis. Nat Methods 9:671-675.

Sultan FA (2013) Dissection of different areas from mouse hippocampus. Bio Protoc 3:e955.

Szklarczyk D, Kirsch R, Koutrouli M, Nastou K, Mehryary F, Hachilif R, Gable AL, Fang T, Doncheva NT, Pyysalo S, Bork P, Jensen LJ, von Mering C (2023) The STRING database in 2023: protein-protein association networks and functional enrichment analyses for any sequenced genome of interest. Nucleic Acids Res 51:D638-646.

Ureña-Peralta JR, Alfonso-Loeches S, Cuesta-Diaz CM, García-García F, Guerri C (2018) Deep sequencing and miRNA profiles in alcohol-induced neuroinflammation and the TLR4 response in mice cerebral cortex. Sci Rep 8:15913.

Vaka R, Parent S, Risha Y, Khan S, Courtman D, Stewart DJ, Davis DR (2023) Extracellular vesicle microRNA and protein cargo profiling in three clinical-grade stem cell products reveals key functional pathways. Mol Ther Nucleic Acids 32:80-93.

Wang L, Hauenstein AV (2020) The NLRP3 inflammasome: Mechanism of action, role in disease and therapies. Mol Aspects Med 76:100889.

Wang Y, Han B, Wang Y, Wang C, Zhang H, Xue J, Wang X, Niu T, Niu Z, Chen Y (2020) Mesenchymal stem cell-secreted extracellular vesicles carrying TGF-β1 up-regulate miR-132 and promote mouse M2 macrophage polarization. J Cell Mol Med 24:12750-12764.

Wu T, Hu E, Xu S, Chen M, Guo P, Dai Z, Feng T, Zhou L, Tang W, Zhan L, Fu X, Liu S, Bo X, Yu G (2021) clusterProfiler 4.0: A universal enrichment tool for interpreting omics data. Innov Camb Mass 2:100141.

Xu F, Wu Y, Yang Q, Cheng Y, Xu J, Zhang Y, Dai H, Wang B, Ma Q, Chen Y, Lin F, Wang C (2022) Engineered extracellular vesicles with SHP2 high expression promote mitophagy for Alzheimer's disease treatment. Adv Mater Deerfield Beach Fla 34:e2207107.

Yin K, Wang S, Zhao RC (2019) Exosomes from mesenchymal stem/stromal cells: a new therapeutic paradigm. Biomark Res 7:8.

Zheng D, Liwinski T, Elinav E (2020) Inflammasome activation and regulation: toward a better understanding of complex mechanisms. Cell Discov 6:36.

C-Editor: Zhao M; S-Editor: Li CH; L-Editors: Li CH, Song LP; T-Editor: Jia Y

Additional Table 1 Primer sequences of the analyzed genes used for quantitative PCR

Gene	Primer sequences (5’ to 3’)
NLRP3	F: AAGTCCTGCCCCAAGCCCCA
	R: GGAAGGGCAGCCTCTGGCAG
Caspase-1	F: GGCACATTTCCAGGACTGACTG
	R: GCAAGACGAGTACGAGTGGTTG
ASC	F: GCTTACAGGAGCTGGCTGAG
	R: TGTGACCCTGGCAATGAGT
IL-1β	F: GACCCCAAAAGATGAAGGGCT
	R: TGTGCTGCTGCGAGATTTGA
IL-18	F: ACTGTACAACCGCAGTAATACGG
	R: AGTGAACATTACAGATTTATCCC
NLRP1	F: TCCAAGAGAGGGTCCACTGA
	R: CCTTGCTGAAACCAGGAGAC
AIM2	F: GTCACCAGTTCCTCAGTTGTG
	R: TGTCTCCTTCCTCGCACTTT
NLRC4	F: TGATGCTGCCTTGGTGCT
	R: ATCCGTCACTGCTCACACAG
Caspase-11/4	F: CCGAGACAAAACAGGAGGC
	R: GGTGGGCATCTGGGAATGA
IRAK1	F: GGACTTCCACAGTTCGAGGTAC
	R: GGTCTTTGCACCTTGTGTCCTC
iNOS	F: AATCTTGGAGCGAGTTGTGG
	R: ATCTCTGCCTATCCGTCTCG
NF-κB	F: TACCCTCAGAGGCCAGAAGA
	R: CAGTTCCGTAGGGATCATCG
CX3CL1	F: TGCGAAATCATGTGCGACAA
	R: TGGACCCATTTCTCCTTCGG
MCP-1	F: AGGTCCCTGTCATGCTTCTG
	R: TCTGGACCCATTCCTTCTTG
TLR4	F: TGCCTCTCTTGCATCTGGCTGG
	R: CTGTCAGTACCAAGGTTGAGAGCTGG
Cyclophilin A	F: GTCTCCTTCGAGCTGTTTGC
	R: GATGCCAGGACCTGTATGCT
snRNA U6	F: GCTTCGGCAGCACATATACTAAAAT
	R: CGCTTCACGAATTTGCGTGTCAT

AIM2: absent in melanoma 2; ASC: apoptosis-associated speck-like protein containing a CARD; CX3CL1: C-X3-C motif chemokine ligand 1 or fractalkine; F: forward; IL: interleukin; iNOS: inducible nitric oxide synthase; MCP-1: monocyte chemoattractant protein-1; NF-κB: nuclear factor-kappa B; NLRC4: caspase recruitment domain-containing 4; NLRP1: pyrin domain-containing 1; NLRP3: NOD-, LRR- and pyrin domain-containing protein 3; R: reverse; TLR4: Toll-like receptor 4.

Additional Table 2 Nucleotide sequences of the primers used for quantitative PCR of microRNAs

MicroRNA	Chromosome location	Accession number #	Mature primer sequences (5' to 3')
mmu-mir-21a-5p	Chr.17: 59841266 – 59841337 [+] on Build GRCh38	MIMAT0000530	UAGCUUAUCAGACUGAUGUUGA
mmu-mir-141a-5p	Chr.6: 124717914 – 124717985 [-] on Build GRCm38	MIMAT0004533	CAUCUUCCAGUGCAGUGUUGGA
mmu-mir-146a-5p	Chr.5: 160485352 – 160485450 [+] on Build GRCh38	MIMAT0000158	UGAGAACUGAAUUCCAUGGGUU

Accession numbers are available from http://mirbase.org/